JACS
JOURNAL OF THE AMERICAN CHEMICAL SOCIETY

Communication

pubs.acs.org/JACS

Cobalt-Modified Porous Single-Crystalline $LaTiO_2N$ for Highly Efficient Water Oxidation under Visible Light

Fuxiang Zhang,[†,‡] Akira Yamakata,[§,⊥] Kazuhiko Maeda,[†,⊥] Yosuke Moriya,[†] Tsuyoshi Takata,[†] Jun Kubota,[†] Katsuya Teshima,[∥] Shuji Oishi,[∥] and Kazunari Domen*[,†]

[†]Department of Chemical System Engineering, School of Engineering, The University of Tokyo, 7-3-1 Hongo, Bunkyo-ku, Tokyo 113-8656, Japan

[‡]State Key Laboratory of Catalysis & Dalian National Laboratory for Clean Energy, Dalian Institute of Chemical Physics, Chinese Academy of Sciences (CAS), 457 Zhongshan Road, Dalian 116023, China

[§]Graduate School of Engineering, Toyota Technological Institute, 2-12-1 Hisakata, Tempaku, Nagoya 468-8511, Japan

[⊥]Precursory Research for Embryonic Science and Technology (PRESTO), Japan Science and Technology Agency (JST), 4-1-8 Honcho Kawaguchi, Saitama 332-0012, Japan

[∥]Department of Environmental Science and Technology, Faculty of Engineering, Shinshu University, 4-17-1 Wakasato, Nagano 380-8553, Japan

Supporting Information

ABSTRACT: Highly efficient water oxidation utilizing visible photons of up to 600 nm is a crucial step in artifical photosynthesis. Here we present a highly active photocatalyst for visible-light-driven water oxidation, consisting of single-crystalline meso- and macroporous $LaTiO_2N$ (LTON) with a band gap of 2.1 eV, and earth-abundasnt cobalt oxide (CoO_x) as a cocatalyst. The optimized CoO_x/LTON had a high quantum efficiency of 27.1 ± 2.6% at 440 nm, which substantially exceeds the values reported for previous particulate photocatalysts with a 600-nm absorption edge.

Water oxidation involving a four-electron transfer is a critically challenging step in artificial photosynthesis for solar fuel production, i.e., water splitting into hydrogen and oxygen, or the reduction of CO_2 to methanol or hydrocarbons.[1] So far, light-driven water oxidation has attracted significant attention in both homogeneous and heterogeneous systems, but the lack of molecular catalysts for the homogeneous process has limited its progress.[2] Comparatively, heterogeneous photocatalysts are more plentiful, and both photoelectrochemical[3] and photocatalytic[4] systems have been demonstrated. Since the powder-based photocatalytic methods only require a water pool containing photocatalyst powders, their simplicity and scalability provide an opportunity for solar energy storage on a terrestrial scale.[4d]

To efficiently store solar energy as chemical energy, a photocatalytic system requires not only the capability to harvest visible photons, which are the main component of the solar spectrum, but also a high quantum efficiency. As discussed in our previous report,[5] a photocatalyst with visible light absorption above 600 nm and a quantum efficiency of ~30% is required for practical application. However, this is presently a distant target. Narrowing the band gap of a photocatalyst increases its absorption of visible light but decreases the driving force for redox reactions. As a consequence, visible-light-driven water splitting generally has low quantum efficiencies for water reduction and oxidation compared to those of oxide photocatalysts with relatively large band gaps (>3 eV). This is a more serious concern in water oxidation than in water reduction in terms of kinetics, because water oxidation involves a complicated four-electron process. To date, reproducible visible-light-responsive materials for overall water splitting are very limited,[6] and there remains a need to improve the efficiency of 600-nm-responsive semiconductor materials, even for half-reactions. Accordingly, efforts to improve the quantum efficiencies of water splitting, especially water oxidation, are very important and necessary to achieve overall water splitting under ≤600 nm light irradiation.

The quantum efficiencies for water splitting in a powder photocatalytic system are primarily affected by the structures of the photocatalyst and cocatalyst.[4a] Generally, the structure of a photocatalyst determines the generation and transfer of carriers (electrons and holes) to the photocatalyst surface. Photocatalyst features such as high crystallinity, low defect density, short charge-transfer distance, large surface area, and special morphology usually enhance the photocatalytic performance.[4a,7] On the other hand, the cocatalyst plays a crucial role in promoting the separation of electrons and holes and provides active sites for H_2 and O_2 evolution.[4a,5] So far, various noble metals have been reported to act as effective cocatalysts for water reduction, while RuO_2 and IrO_2 have shown comparatively better performance as cocatalysts for water oxidation. Thus, comprehensive consideration of various factors involving a photocatalyst and a cocatalyst is the key to developing a photocatalytic material with a high quantum efficiency for water splitting. It is also important that the photocatalytic system uses cheap, earth-abundant metals in order to produce solar fuel on a large scale.[8]

The oxynitride $LaTiO_2N$ (LTON) is an n-type semiconductor material with a perovskite structure and a band

Received: February 21, 2012
Published: May 8, 2012

dx.doi.org/10.1021/ja301726c | J. Am. Chem. Soc. 2012, 134, 8348−8351

gap of 2.1 eV (~600 nm absorption edge). For solar water splitting, LTON not only has favorable energy band positions but also is composed of relatively cheap elements. Using this material, visible-light-driven water splitting for H_2 or O_2 production in the presence of sacrificial reagents has been demonstrated to be theoretically and experimentally feasible in our previous work.[9] Although a quantum efficiency of ~5% for water oxidation has been achieved using IrO_2-loaded LTON,[9a] the efficiency must be further improved, and the precious cocatalyst IrO_2 should be replaced with a more earth-abundant metal species.

Here, we show that the low quantum efficiency of visible-light-driven water oxidation on LTON can be addressed by suitably modifying both the photocatalyst and cocatalyst components. Oxide precursors ($La_2Ti_2O_7$) prepared by a flux method and the polymerized complex (PC) method were subjected to heat treatment under a flow of NH_3 at 1223 K. The as-nitrided powders are referred to as FX-LTON and PC-LTON, respectively. Cobalt oxide (CoO_x) was deposited on LTON samples as a cocatalyst for water oxidation by an impregnation method from aqueous $Co(NO_3)_2$ solution, followed by NH_3 treatment at 973 K and calcination at 473 K in air. The preparation details are described in the Supporting Information.

Figure 1 displays various characterization results of the as-prepared FX-LTON sample. Single-phase well-crystallized

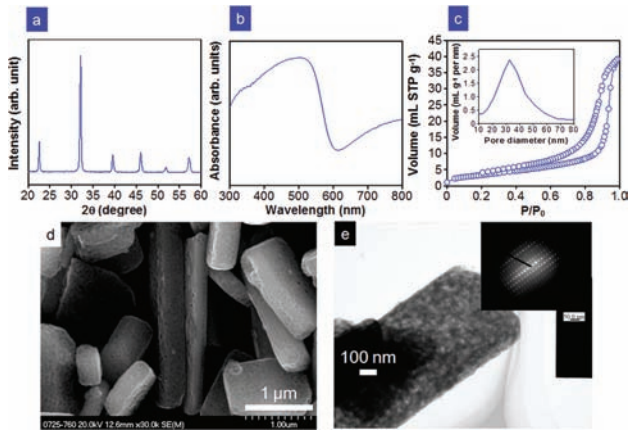

Figure 1. Various characterizations of an FX-LTON sample: (a) XRD patterns; (b) UV–vis spectra; (c) adsorption–desorption isotherms and pore size distribution (inset); (d) SEM image; (e) HR-TEM image and SAED patterns (inset).

LTON particles with a visible absorption band of ~600 nm were indicated from the XRD patterns and UV–vis spectrum shown in panels a and b of Figure 1, respectively. The nitrogen adsorption–desorption isotherms of the sample given in Figure 1c were typical type-IV adsorption isotherms for a porous material, indicating the existence of a pore structure. The capillary condensation step in the adsorption branch was observed at relatively high pressure, indicating a large pore diameter. The specific surface area determined by nitrogen adsorption at 77 K was ~16 $m^2 \cdot g^{-1}$. The pore size distribution (inset in Figure 1c) determined from the corresponding desorption branch using the BJH method was very broad, ranging from 10 to 80 nm, indicating existence of both mesoporous and macroporous structures. The mean pore size was 28.3 nm.

The mesoporous and macroporous architectures were confirmed by the SEM and HR-TEM images shown in panels d and e of Figures 1, respectively. In Figure 1d, well-dispersed brick-like LTON particles with a porous structure were clearly observed, and the surface of the particles was mostly smooth, with a few of them carrying attached nanoparticles. Selected-area electron diffraction (SAED, see inset in Figure 1e) and HR-TEM images (Figure 1e) taken from a single particle further demonstrated that the as-obtained LTON particle was a single-crystalline porous material. To the best of our knowledge, this is the first example of a quaternary oxynitride with both mesoporous and macroporous architectures.

The morphology and structure of the FX-LTON sample were obviously different from those of PC-LTON synthesized from an amorphous oxide precursor. The X-ray diffraction peaks of the oxide precursors in Figure S1A are distinct, but a single phase of LTON particles was observed in both as-nitrided oxynitrides (Figure S1B). Comparatively, the relative diffraction intensities of the FX-LTON sample were slightly higher than those of PC-LTON, demonstrating better crystallinity. Aggregated nanoparticles without pore structures (see Figure S2) were mainly observed in the PC-LTON sample, unlike the brick-like pore structure of the FX-LTON sample. As seen in Figure S3, both samples had similar absorption edges of ~600 nm, but the FX-LTON sample had a lower absorption background, which indicates a lower density of defects derived from Ti^{3+} species formed.

For use in photocatalytic water oxidation, cobalt species were deposited onto the as-prepared LTON samples by a simple impregnation method from an aqueous $Co(NO_3)_2$ solution, followed by heat-treatment with NH_3. The cobalt species deposited on the surface of the FX-LTON sample was analyzed by XPS. As shown in Figure S4, the resulting Co $2p_{3/2}$ and $2p_{1/2}$ peaks, located at 781.1 and 796.8 eV, respectively, were in good agreement with the positions of both Co(II) and Co(III) reported in the literature,[10] and the satellite peak at 787.7 eV is a characteristic feature of Co^{2+} ions. The existence of cobalt oxide on the surface of the FX-LTON sample was further confirmed by the HR-TEM micrograph shown in Figure 2, in

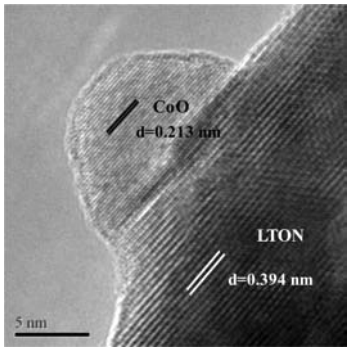

Figure 2. HR-TEM image of a CoO_x/FX-LTON sample.

which the (200) crystal face of CoO nanoparticles 5 nm in size can be judged according to the lattice spacing of the fringes (d = 0.213 nm). As seen in Figure S5, aggregated cobalt oxide nanoparticles were also observed, with the lattice spacing of the fringes (d = 0.165, 0.202, and 0.213 nm) that correspond to the (422) and (400) crystal faces of Co_3O_4 and the (200) face of CoO, respectively. Since the deposited cobalt oxide species

dx.doi.org/10.1021/ja301726c | J. Am. Chem. Soc. 2012, 134, 8348–8351

contained both Co(II) and Co(III), they are referred to as CoO_x hereafter for simplicity.

The water oxidation performance of a CoO_x-modified FX-LTON sample under visible light irradiation was examined in the presence of silver nitrate as an electron acceptor. The reproducibility of the rate of O_2 evolution was within ~10% under the same reaction conditions. First, the cobalt loading was optimized. As shown in Figure S6, the rate of O_2 evolution on the CoO_x/FX-LTON catalysts was strongly dependent on the cobalt loading, and the promotional effect of deposited CoO_x was clearly demonstrated. Without loading, the FX-LTON sample showed a moderate rate of O_2 evolution (~25 μmol·h^{-1}), while a cobalt loading of only 0.01 wt% on FX-LTON led to an ~8-fold enhancement in activity. With increasing cobalt deposition, the rate of O_2 evolution on CoO_x/FX-LTON was further enhanced, reaching a maximum value of ~736 μmol·h^{-1} at a cobalt loading of 2 wt%. The optimal rate of O_2 evolution was ~30 times that of the original sample without cobalt deposition. The pH value of the solution after photocatalytic reaction was slightly decreased from 8.5 to ~8.0 because of the oxidation of OH^- in water, similar to previous observation.[9b]

Table 1 further compares the visible-light-driven catalytic performance of water oxidation on several LTON samples with different cocatalysts. For the FX-LTON catalyst (entities 1−4), cocatalyst loading obviously enhanced the rate of oxygen evolution to different extents, and CoO_x was found to be the most efficient. IrO_2, which is well known as one of the most efficient water oxidation cocatalysts, also resulted in a marked enhancement in the water oxidation activity of LTON samples. However, IrO_2 was not as effective as CoO_x, regardless of the LTON preparation method, even though the loading amount of IrO_2 was optimized. Furthermore, FX-LTON gave a higher performance than PC-LTON, regardless of the cocatalyst employed (entries 3−6). This higher activity of FX-LTON can be attributed at least in part to the single-crystalline texture with mesoporous and microporous architecture inside the LTON particles. Compared to the PC-LTON sample, the well-crystallized porous FX-LTON photocatalyst not only provided more active surface area but also had a lower defect density, which would inhibit recombination of photogenerated carriers. In addition, one control experiment demonstrated that thermal treatment of LTON with NH_3 alone (without cobalt coating) did not promote photocatalytic activity of water oxidation (entry 2), clearly demonstrating that the enhancement of activity is attributed to the deposited CoO_x nanoparticles.

Table 1. Influence of Cocatalysts on the O_2 Evolution of FX-LTON and PC-LTON Photocatalysts[a]

entry	catalyst (specific surface area)	cocatalyst	O_2 evolution rate/ μmol·h^{-1}
1	FX-LTON (16 m^2·g^{-1})	none	25
2		none[b]	15
3		2 wt% CoO_x	736
4		2 wt% IrO_2	170
5	PC-LTON (15 m·g^{-1})	2 wt% CoO_x	489
6		2 wt% IrO_2	146
7		none	24

[a]Reaction conditions: catalyst, 0.2 g (0.2 g of La_2O_3 as a buffer); reactant solution, aqueous silver nitrate solution (0.05 M, 200 mL); light source, xenon lamp (300 W) with cutoff filter; reaction vessel, top-irradiation type; 1 h irradiation. [b]The FX-LTON catalyst was treated under NH_3 flow at 973 K for 1 h and postcalcination at 473 K in air for 1 h, but without cocatalyst deposition.

Figure S7 shows detailed time courses of O_2 evolution on the CoO_x-modified LTON samples under visible irradiation (λ > 420 nm). No reaction took place in the dark, and gas evolution began with the onset of irradiation. The rate of O_2 evolution decreased with increasing reaction time because of the decrease in Ag^+ concentration and because more and more of the LTON surface became covered with metallic Ag deposits generated by the reduction of Ag^+, hindering light absorption and decreasing the number of active sites available for reaction. This is a typical behavior observed in photocatalytic water oxidation.[9] The apparent quantum efficiency in the initial 15 min of irradiation was 27.1 ± 2.6% at 440 nm, which is 5−6 times higher than that reported previously using IrO_2/PC-LTON[9a] and is by far the highest value reported value for a particulate photocatalyst with a 600-nm-class absorption band. A low level of N_2 evolution (~2−8 μmol) was detected in the initial stage of the reaction (first 1−2 h) for all of the present samples. This is attributed to the oxidation of N^{3-} species near the LTON surface to N_2, as has been observed for other (oxy)nitride photocatalysts.[4a,9] However, the production of N_2 is completely suppressed as the reaction progresses, indicative of the stability of the material. Recently, a very high quantum yield of photochemical O_2 evolution (~90% at 420−440 nm) was reported for Ag_3PO_4.[11] However, this material only works under irradiation by light with wavelengths shorter than 530 nm. More importantly, the material undergoes self-reductive decomposition under band gap irradiation, producing O_2 from water along with the deposition of Ag on the surface. In contrast to these inherent drawbacks of Ag_3PO_4, LTON with a 600-nm absorption edge acts as a stable photocatalyst for water oxidation without any noticeable change in its structure, as we confirmed in our previous study.[9a] Such a high quantum efficiency had not been previously achieved using a photocatalyst capable of absorbing visible photons of up to 600 nm.

To further investigate this unusual enhancement, several experiments were performed. The effect of CoO_x-loading of LTON on its water oxidation performance was investigated by a photoelectrochemical technique, since LTON is an n-type semiconductor.[9] As shown in Figure S8, a CoO_x-modified electrode generated a much higher anodic photocurrent upon visible light irradiation than an unmodified LTON electrode, with a more negative photocurrent onset potential. This indicates that CoO_x on LTON does indeed promote water oxidation.

To investigate the lifetime of photogenerated carriers in the modified LTON samples, time-resolved infrared absorption (TR-IR) measurements were conducted. A shown in Figure 3, the deposition of both CoO_x and IrO_2 can obviously enhance the lifetime of excited electrons with respect to the original FX-LTON, while the deposited CoO_x prolonged the lifetime of the carriers even more significantly to a time scale of 1 s. Therefore, both CoO_x and IrO_2 play roles in separating the photogenerated electrons and holes, and the better separation of carriers with CoO_x modification explains the higher photocatalytic performance than with IrO_2 modification. Accordingly, the high quantum efficiency of water oxidation can be attributed to both the morphological character of FX-LTON and efficient charge separation followed by water oxidation catalysis by the deposited CoO_x nanoparticles.

dx.doi.org/10.1021/ja301726c | J. Am. Chem. Soc. 2012, 134, 8348−8351

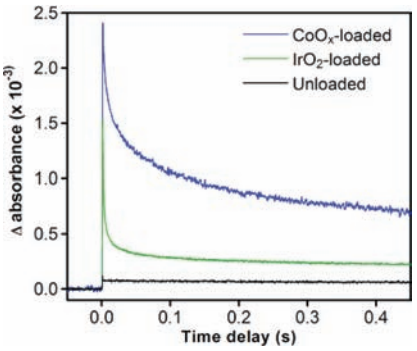

Figure 3. Decay of photogenerated electrons on FX-LTON with and without cocatalysts: (a) FX-LTON; (b) IrO_2/FX-LTON; and (c) CoO_x/FX-LTON. A 355 nm UV pulse at 1 mJ was irradiated on the catalysts, and the transient absorption was observed at 2000 cm^{-1}.

In conclusion, CoO_x-modified $LaTiO_2N$ with both single-crystalline mesoporous and macroporous architectures was shown to achieve high water oxidation performance under visible light irradiation. The significantly enhanced quantum efficiency can be attributed to improvements in both the photocatalyst and cocatalyst components. The observed remarkable promotion of water oxidation can be seen as the first glimmer of a new dawn in overall water splitting on 600-nm-responsive materials.

■ ASSOCIATED CONTENT

Ⓢ Supporting Information

Experimental details and other characterization data of photocatalysts. This material is available free of charge via the Internet at http://pubs.acs.org.

■ AUTHOR INFORMATION

Corresponding Author

domen@chemsys.t.u-tokyo.ac.jp

Notes

The authors declare no competing financial interest.

■ ACKNOWLEDGMENTS

This work was supported by a Grant-in-Aid for Specially Promoted Research (No. 23000009) of the Ministry of Education, Culture, Sports, Science, and Technology (MEXT) of Japan, and Advanced Low Carbon Technology Research and Development Program (ALCA) of the JST. Acknowledgements are also extended to "100 talents program" of DICP, CAS, and the A3 Foresight Program among Japan, Korea, and China. K.M. thanks the Nippon Sheet Glass Foundation for Materials Science and Engineering for funding support. The authors thank Dr. D. Lu (Tokyo Institute of Technology) for measurement of TEM images.

■ REFERENCES

(1) (a) Toma, F. M.; Sartorel, A.; Lurlo, M.; Carraro, M.; Parisse, P.; Maccato, C.; Rapino, S.; Gonzalez, B. R.; Amenitsch, H.; Ros, T. D.; Calalis, L.; Goldoni, A.; Marcaccio, M.; Scorrano, G.; Scoles, G.; Paolucci, F.; Prato, M.; Bonchio, M. *Nat. Chem.* **2010**, *2*, 826. (b) Liu, F.; Concepcion, J. J.; Jurss, J. W.; Cardolaccia, T.; Templeton, J. L.; Meyer, T. J. *Inorg. Chem.* **2008**, *47*, 1727. (c) Barber, J. *Chem. Soc. Rev.* **2009**, *38*, 185. (d) Wang, D.; Jiang, H.; Zong, X.; Xu, Q.; Ma, Y.; Li, G.; Li, C. *Chem.—Eur. J.* **2011**, *17*, 1275.

(2) Concepcion, J. J.; Jurss, J. W.; Brennaman, M. K.; Hoertz, P. G.; Patrocinio, A. O. T.; Iha, N. Y. M.; Templeton, J. L.; Meyer, T. J. *Acc. Chem. Res.* **2009**, *42*, 1954.

(3) (a) Fujishima, A.; Honda, K. *Nature* **1972**, *238*, 37. (b) Youngblood, W. J.; Lee, S. H. A.; Maeda, K.; Mallouk, T. E. *Acc. Chem. Res.* **2009**, *42*, 1966. (c) Sivula, K.; Le Formal, F.; Grätzel, M. *ChemSusChem* **2011**, *4*, 432.

(4) (a) Maeda, K.; Domen, K. *J. Phys. Chem. C* **2007**, *111*, 7851. (b) Kudo, A.; Miseki, Y. *Chem. Soc. Rev.* **2009**, *38*, 253. (c) Inoue, Y. *Energy Environ. Sci.* **2009**, *2*, 364. (d) Wang, X.; Maeda, K.; Thomas, A.; Takanabe, K.; Xin, G.; Carlsson, J. M.; Domen, K.; Antonietti, M. *Nat. Mater.* **2009**, *8*, 76. (e) Iwase, A.; Ng, Y. H.; Ishiguro, Y.; Kudo, A.; Amal, R. *J. Am. Chem. Soc.* **2011**, *133*, 11054.

(5) Maeda, K.; Domen, K. *J. Phys. Chem. Lett.* **2010**, *1*, 2655.

(6) (a) Maeda, K.; Teramura, K.; Lu, D.; Takata, T.; Saito, N.; Inoue, Y.; Domen, K. *Nature* **2006**, *440*, 295. (b) Lee, Y.; Terashita, H.; Shimodaira, Y.; Teramura, K.; Hara, M.; Kobayashi, H.; Domen, K.; Yashima, M. *J. Phys. Chem. C* **2007**, *111*, 1042.

(7) (a) Yang, H. G.; Sun, C. H.; Qiao, S. Z.; Zou, J.; Liu, G.; Smith, S. C.; Cheng, H. M.; Lu, G. Q. *Nature* **2008**, *453*, 638. (b) Noda, Y.; Lee, B.; Domen, K.; Kondo, J. N. *Chem. Mater.* **2008**, *20*, 5361.

(8) (a) Kanan, M. W.; Nocera, D. G. *Science* **2008**, *321*, 1072. (b) Jiao, F.; Frei, H. *Angew. Chem., Int. Ed.* **2009**, *48*, 1841.

(9) (a) Kasahara, A.; Nukumizu, K.; Hitoki, G.; Takata, T.; Kondo, J. N.; Hara, M.; Kobayashi, H.; Domen, K. *J. Phys. Chem. A* **2002**, *106*, 6750. (b) Kasahara, A.; Nukumizu, K.; Takata, T.; Kondo, J. N.; Hara, M.; Kobayashi, H.; Domen, K. *J. Phys. Chem. B* **2003**, *107*, 791.

(10) (a) Jansson, J.; Palmqvist, A. E. C.; Fridell, E.; Skoglundh, M.; Osterlund, L.; Thormahlen, P.; Langer, V. *J. Catal.* **2002**, *211*, 387. (b) Hyman, M. P.; Vohs, J. M. *Surf. Sci.* **2011**, *605*, 383.

(11) Yi, Z.; Ye, J. H.; Kikugawa, N.; Kako, T.; Ouyang, S.; Stuart-Williams, S.; Yang, H.; Cao, J. Y.; Luo, W. J.; Li, Z. S.; Liu, Y.; Withers, R. L. *Nat. Mater.* **2010**, *9*, 559.